

Nanostructured thin films for multiband-gap silicon triple junction solar cells

R.E.I. Schropp*, H. Li, R.H. Franken, J.K. Rath, C.H.M. van der Werf, J.W.A. Schüttauf, R.L. Stolk

Utrecht University, Faculty of Science, SID-Physics of Devices, P.O. Box 80.000, 3508 TA Utrecht, The Netherlands

Available online 16 January 2008

Abstract

By implementing nanostructure in multiband-gap proto-Si/proto-SiGe/nc-Si:H triple junction n–i–p solar cells, a considerable improvement in performance has been achieved. The unalloyed active layers in the top and bottom cell of these triple junction cells are deposited by Hot-Wire CVD. A significant current enhancement is obtained by using textured Ag/ZnO back contacts instead of plain stainless steel. We studied the correlation between the integrated current density in the long-wavelength range (650–1000 nm) with the back reflector surface roughness and clarified that the *rms* roughness from 2D AFM images correlates well with the long-wavelength response of the cell when weighted with a Power Spectral Density function. For single junction 2- μm thick nc-Si:H n–i–p cells we improved the J_{sc} from 15.2 mA/cm² for plain stainless steel to 23.4 mA/cm² using rough back reflector. We introduced profiling of the H₂ dilution during growth of the nc-Si:H layer to prevent a transition to amorphous growth. The efficiency for a single junction n–i–p cell reached 8.5%, the highest reported value for HWCVD cells of this kind. Moreover, these cells show to be totally stable under light-soaking tests. Combining the above techniques, an efficiency of 10.9% has been obtained for triple junction cells (J_{sc} =8.35 mA/cm², V_{oc} =1.98 V, FF=0.661). By using effective light trapping techniques and three different band-gap materials, the required thickness could be kept small (~2.5 μm total).

© 2007 Elsevier B.V. All rights reserved.

Keywords: Solar cells; Light scattering; Nanostructure; Nanocrystalline silicon; Multijunction; Efficiency; Stability

1. Introduction

Amorphous silicon (a-Si:H) and nanocrystalline (or microcrystalline) silicon (nc-Si:H or $\mu\text{c-Si:H}$) are conventionally produced by plasma-enhanced chemical vapor deposition (PECVD). This technique is based on the dissociation of silicon-containing gases (usually silane (SiH₄) and hydrogen (H₂)) in a radiofrequency (rf) plasma, usually at a frequency of 13.56 MHz. During the last few decades, the plasma deposition parameter regime has been explored intensively [1–3] in order to improve materials and increase the deposition rate, specifically for nc-Si:H. The favored formation of nanocrystallites occurs under plasma conditions close to the transition regime [4]. In this regime, which is characterized by high pressure, high power, large inter-electrode distance, and low substrate temperature, secondary reactions are promoted. Unfortunately, this regime is close to that where unwanted powder formation occurs.

A technique that is not plasma based is Hot-Wire CVD (HWCVD), which is based on catalytic decomposition of SiH₄ and H₂ gases on a hot filament. Because source gases are catalytically decomposed, the method is often referred to as thermo-catalytic CVD (TCCVD) [5] or catalytic CVD (Cat-CVD) [6]. The HWCVD technique has been shown to be a viable method for the deposition of silicon-based thin films and solar cells [7–10]. This technique can be considered to be a remote technique, since it is based on the decomposition of silicon-containing gases at a catalytic hot surface, while the substrate itself has no active role in generating the active precursors, unlike the case of PECVD where it usually has at least a role as the grounded electrode. The absence of the requirement to achieve an equipotential plane at the substrate makes it easier to transport either rigid or foil type substrate materials during deposition and to scale up to large areas.

The technology of Hot-Wire Chemical Vapor Deposition or Catalytic CVD has made great progress during the last couple of years. Novel materials have been obtained with controlled properties and there is increasing evidence that large area continuous coating is feasible. This review discusses a number of examples of significant progress at our laboratory. Specifically,

* Corresponding author. Tel.: +31 30 2533170; fax: +31 30 2543165.

E-mail address: r.e.i.schropp@phys.uu.nl (R.E.I. Schropp).

recent single junction and multijunction n–i–p type solar cells are highlighted.

We have developed HWCVD intrinsic protocrystalline silicon (proto-Si:H), which is characterized by an enhanced medium range structural order and a higher stability against light-soaking [11] compared to amorphous silicon, and nanocrystalline silicon (nc-Si:H), with a low density of states [12] at a Raman crystalline ratio of $\sim 40\%$. These materials were successfully applied in thin film solar cells on plain stainless steel [13,14]. To enhance the efficiency, multiband-gap structures are required [15]. To this end, we first developed proto-Si/nc-Si/nc-Si triple junction cells, but it appeared that the intrinsic absorber layers have to be made extremely thick in order to match the currents generated in the respective subcells. We therefore implemented three modifications to our cell design. First, the nc-Si:H absorber layer of the middle cell was replaced by a plasma-enhanced chemical vapor-deposited (PECVD) protocrystalline silicon-germanium (proto-SiGe:H) layer, which is highly stable against light-soaking [16]. This allows for more efficient spectral splitting and thus higher solar cell efficiency. The wider band-gap of proto-SiGe:H increases the open-circuit voltage (V_{oc}).

Second, a textured back reflector (TBR) was incorporated in the cell to improve the short-circuit current density (J_{sc}). As a part of this step, the n-layer deposition of the nc-Si:H bottom cell was re-optimized. Thirdly, the n/i-interface and i-layer of the bottom cell were profiled to improve its performance [17].

A schematic picture of the triple junction cell structure is shown in Fig. 1. In the present paper, we report recent results for the improved single junction nc-Si:H bottom cell and the triple junction cell including the stability of these cells under light-soaking.

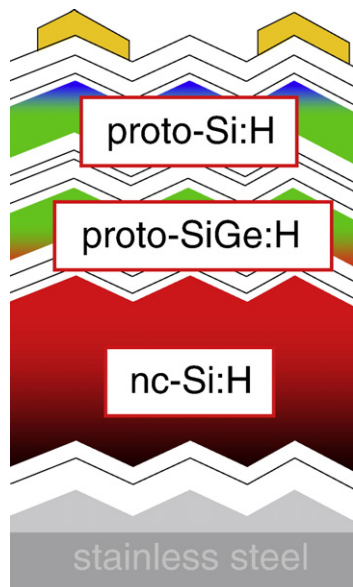


Fig. 1. Schematic cross-section of a triple junction thin film solar cell deposited onto a stainless steel substrate with a textured back reflector. The different subcell absorber materials are nc-Si:H, proto-SiGe, and proto-Si (from bottom to top). On top of the silicon layers is an indium tin oxide/gold contact. The layers that remain unfilled (white) are doped layers, buffer layers, ITO, and ZnO layers.

2. Experimental details

The silicon layers of the n–i–p structured solar cells were deposited in the PASTA multi-chamber ultra-high vacuum system. Details of the cell structures can be found in previous publications [14,18,19]. Doped layers and intrinsic proto-SiGe:H [19] were prepared using 13.56 MHz PECVD, whereas HWCVD was applied to fabricate intrinsic proto-Si:H [13] and nc-Si:H [15,20]. For all hot-wire depositions, two straight Ta filaments with a diameter of 0.5 mm were used, through which a current of 10.5 A was passed, yielding a wire temperature of 1850 °C (vacuum calibration). The calibrated substrate temperature was 250 °C on 1 mm glass substrates. Proto-Si:H was deposited from undiluted SiH₄, at a pressure of 0.02 mbar, whereas H₂-diluted SiH₄ with a H₂ dilution (H₂-flow/total gas flow) of around 0.95, at 0.05 mbar, was used for nc-Si:H deposition. The deposition rates were 10 Å/s and 2.1 Å/s for proto-Si:H and nc-Si:H, respectively. The proto-Si:H is characterized in that it has enhanced medium range order but no Raman-distinguishable nanocrystallites [11]. A fingerprint of the protocrystalline nature of this material is the narrow width of the first sharp peak in X-ray diffraction (XRD) [21]. The nc-Si:H is a so-called mixed phase or transition material, consisting of nanocrystallites in an a-Si:H matrix [13,19]. The Raman ratio of crystallinity for this material is 40% and the crystallites have 10–20 nm sizes [22].

Two types of substrates were used: a Ag/ZnO TBR made on stainless steel (SS) foil in our laboratory and a SS/Ag/ZnO substrate provided by United Solar Ovonic LLC Corporation, for comparison. Indium–tin–oxide served as an anti-reflecting TCO top window; an evaporated gold grid on top facilitated a proper charge carrier collection. Both the metal oxide layers and the textured Ag of the TBR were deposited by rf magnetron sputtering in our SALS system. The active area of the solar cells was 0.13 cm².

The proto-SiGe:H was optimized on textured Asahi U-type SnO₂:F substrates conformally coated with Ag and ZnO to provide a constant-quality textured back contact.

3. Thin film nc-Si:H n–i–p cells

By using a rough, scattering back contact, the light absorption, and thus the photogenerated current density, in the n–i–p configuration can be considerably enhanced. To this end, we developed textured Ag/ZnO:Al back reflector layers on stainless steel substrates, using rf magnetron sputtering. An example of the surface morphology as observed with Scanning Electron Microscopy (SEM) is shown in Fig. 2. This figure shows three identical Ag layers, magnetron sputtered from a 99.99% pure Ag target onto a substrate held at 400 °C, without ZnO:Al (a), with 100 nm ZnO:Al (b) and with 1000 nm ZnO:Al (c), respectively. The ZnO:Al layer is sputtered from a ZnO:Al (1%) target at 80 °C substrate temperature. It is clearly visible that the roughness decreases with increasing ZnO thickness.

We studied the correlation between the integrated current density in the long-wavelength range (650–1000 nm) with the back reflector surface roughness and it became clear that the

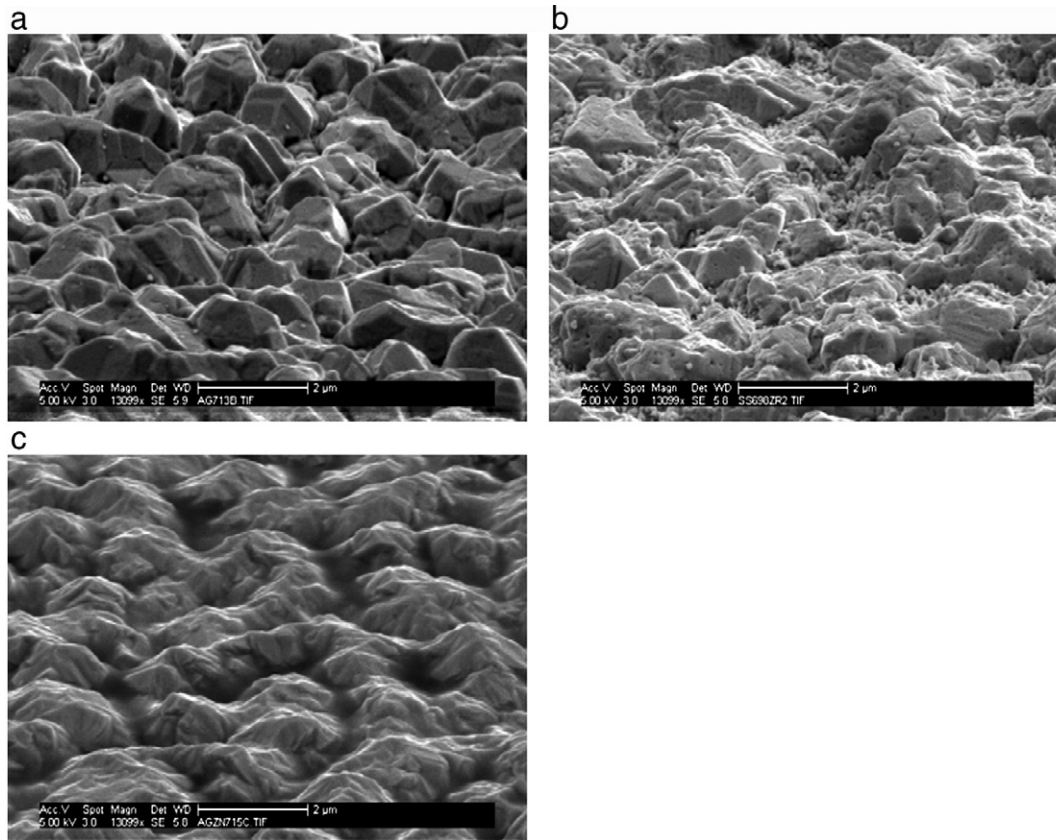


Fig. 2. SEM pictures of rough Ag layers on stainless steel; deposition temperature 400 °C, a) uncoated, b) coated with 100 nm ZnO:Al, and c) coated with 1.0 μm ZnO:Al.

rms roughness from 2D AFM images correlates well with the long-wavelength response of the cell when weighted with a Power Spectral Density (PSD) function that gives the lateral features with dimensions similar to the effective wavelength to be scattered a larger weight [23,24]. A property that limits the optical performance of the back reflector is its plasmon absorption. Although the high-energy surface plasmon absorption band is not directly detrimental to the cell performance, the high microscopic roughness of the Ag shifts the parasitic absorption far into the visible spectrum, leading to a reflectance deficit that does negatively affect the current generation. The correlation between surface morphology and generated current improves if this is taken into account. Fig. 3 shows the correlation between the external collection efficiency, integrated from 650 to 1000 nm, corrected for plasmon-induced losses, versus the *rms* roughness, weighted using PSD functions.

It can be seen in Fig. 3 that the long-wavelength ECE correlates well with the weighted *rms* roughness and that it shows saturation at high weighted *rms* values. The saturated current of 11 mA/cm² is the current generated by light in the 650 to 1100 nm region, and is still not as large as the optical limit given by the number of photons in this region. Nevertheless, for single junction 2-μm thick nc-Si:H n-i-p cells we improved the short-circuit current density (for AM1.5 100 mW/cm² illumination) from the value of 15.2 mA/cm² for plain stainless steel to 23.4 mA/cm² for stainless steel coated with a textured Ag/ZnO back reflector [24].

Fig. 4 shows the comparison between the spectral response curves of an optimized single junction nc-Si:H cell on a textured back contact and that of a cell with an equally thick i-layer (2.0 μm) on plain stainless steel. It is clear that the response of the cell on the textured back contact is higher over the entire wavelength region studied. The enhancement at long wavelengths is as expected, due to efficient light trapping within

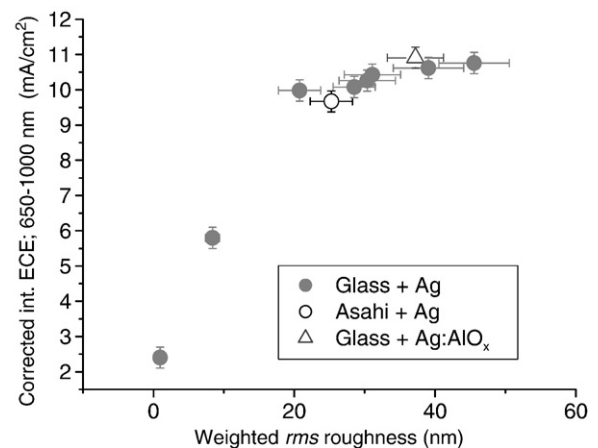


Fig. 3. The correlation between the plasmon corrected long-wavelength generated current density of nc-Si:H n-i-p cells and the weighted *rms* roughness for a large variety of back reflector morphologies.

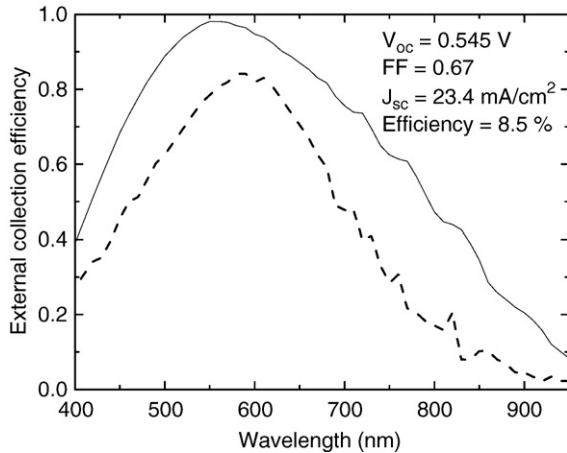


Fig. 4. Spectral response of a cell on plain stainless steel (dashed curve; generating 15.6 mA/cm^2) and an optimized cell on a textured Ag/ZnO:Al back contact (solid curve; generating 23.4 mA/cm^2). The cells have equally thick i-layers ($2 \mu\text{m}$ HWCVD nc-Si:H).

the cell. The enhancement at shorter wavelengths is a result of the roughness of the total cell structure. The top surface of the cell partially mimics the roughness of the back contact. Due to this effect, the front contact also has some roughness. This leads to an effective gradient in the refractive index from air to ITO, due to which reflection losses at short wavelengths are reduced and a higher response is obtained in this region as well.

Table 1 shows the present cell results in comparison with other data obtained on single junction nc-Si:H n-i-p type cells on various substrates [15,25–28]. The table also includes the latest best results obtained at United Solar Ovonic, LLC, for n-i-p type cells as obtained using their ‘modified VHF’ technique. We believe that the obtained efficiency of 8.5% is a record value for hot-wire deposited nc-Si:H n-i-p cells. Further, the deposition rate of 2.1 \AA/s is about twice as high as in record HWCVD deposited cells so far [29,30]. Moreover, when this cell is light soaked at a temperature of $50 \text{ }^\circ\text{C}$, the cell shows to be totally stable (relative efficiency loss $\Delta\eta/\eta < 0.6\%$ after 500 h of light-soaking).

The growth of microcrystalline silicon layers near the a-Si:H/nc-Si:H phase transition regime with HWCVD shows a different trend in the thickness direction than plasma-enhanced CVD deposited layers. When the hydrogen dilution ratio and the

filament current is kept constant during deposition, the material evolves from microcrystalline into an amorphous network [20], rather than into a microcrystalline structure with higher crystallinity as has been observed quite generally for nc-Si:H growth by plasma-enhanced CVD. There are several possible reasons for the observed microcrystalline to amorphous transition during HWCVD growth. One possible reason is the strongly different growth dynamics at the film surface, due to the complete absence of energetic ions in HWCVD, leaving the growing surface free from any ion bombardment. Another reason might be a gradual change in the reactivity of the filament surface due to accumulation of silicon or silicides on the filament if the filament current is kept unchanged during the entire deposition time. The third reason may be that the structural evolution of the growing film is strongly influenced by the nature of the substrate or a layer that is already present. In the present case, the nanocrystalline nature of the n^+ layer may induce immediate nucleation of nanocrystallites in the i-layer while under prevailing growth conditions nanocrystalline growth is not maintained during growth of the bulk of the film. These three effects may side-by-side result in the anomalous trend in nanocrystalline development during deposition, especially for conditions near the phase transition regime.

This led us to stepwise increase the H_2 dilution during growth in order to maintain a constant crystalline volume fraction and prevent the transition to amorphous growth [17]. A further minor improvement is obtained by using a ‘dynamic start’, which means that the deposition is started before the substrate reaches its equilibrium temperature. In this mode, the substrate temperature increases while the i-layer grows thicker. Presently, we are investigating the origin of the structural evolution and using filament monitoring and control schemes to dynamically adjust the filament current such that homogeneous growth over the entire thickness is maintained.

4. Thin film nc-Si:H n-i-p triple junction cells

The results on single junction nc-Si:H cells have been utilized in triple junction n-i-p type cells. Previously, we have been optimizing triple junction cells of the type proto-Si/nc-Si:H/nc-Si:H, comprising active i-layers that were all deposited by HWCVD. In order to obtain sufficient current, however, this design leads to the use of very thick absorber layers, even when enhanced scattered back reflection is applied. For instance, if the top cell is 165 nm in order to generate $\sim 8 \text{ mA/cm}^2$, the middle cell and the bottom cell have to be made as thick as $\sim 2.4 \mu\text{m}$ and $\sim 3.7 \mu\text{m}$, respectively. The total thickness of over

Table 1
Present status of single junction HWCVD nc-Si:H n-i-p solar cells at various laboratories

Laboratory [ref]	V_{oc} (V)	J_{sc} (mA/cm^2)	FF	η (%)
Utrecht [present work]	0.545	23.39	0.668	8.52
Jülich [25]	0.542	19.9	0.69	7.5
Kaiserslautern [26]	0.522	21.6	0.66	7.3
Ecole Polytechnique [27]	0.42	20.7	0.59	5.1
Gifu [28]	0.550	11.32	0.56	3.49
Unisolar [15] (non-HWCVD)	0.568	23.59	0.671	8.99

Table 2
 J - V parameters of the best microcrystalline single junction and triple cells

Type of cell	V_{oc} (V)	FF	J_{sc} (mA/cm^2)	Efficiency (%)
Single junction nc-Si:H n-i-p	0.55	0.66	23.4	8.5
Triple junction proto-Si/proto-SiGe:H/nc-Si:H	1.98	0.66	8.35	10.9

6 μm of nc-Si:H material is very large compared to the micromorph tandem concept and it would take too much deposition time (at the present deposition rate) to economically produce such triple cells.

However, if the nc-Si:H middle cell is replaced by a proto-SiGe:H cell, then not only the middle cell can be made an order of magnitude thinner, but also the bottom nc-Si:H cell can be made considerably thinner, since the SiGe:H middle cell does not absorb light from exactly the same spectral region. A second important advantage is that a higher V_{oc} of the triple cell can be obtained, because SiGe:H has a higher band-gap than nc-Si:H. Thirdly, in principle the achievable conversion efficiency is higher, because all three band-gaps are different and less photon energy is lost as heat. We use PECVD for the deposition of the middle cell, since it was readily available in our lab. The SiGe:H middle cell can be made by HWCVD as well, as is demonstrated by the good single junction cell results obtained by NREL [31].

The efficiency reached for proto-Si/proto-SiGe/nc-Si:H triple junction n-i-p solar cells on a textured Ag/ZnO coated stainless steel substrate is 10.9%. Table 2 shows the parameters of the single junction and the triple junction n-i-p solar cells.

Fig. 5 gives the spectral response data of the triple junction cell. It is worth noting that the three silicon cells stacked on top of each other are together approximately 2.5 μm thick.

Single junction and triple junction cells have been exposed to light-soaking under open-circuit conditions and a temperature of 50 $^{\circ}\text{C}$. Fig. 6a shows the degradation kinetics of the single junction cell and Fig. 6b that of a bottom cell limited triple cell.

We found that the relative degradation of the nc-Si:H n-i-p cell is negligible (0.6%), while that of the triple cell is 3.5%. It is noted that while the initial efficiency of the triple cell is not at a world record level, the stability of it is excellent. There is an additional economical advantage since the thickness of the entire stack of silicon films is only 2.5 μm .

For a multitude of cells on the same substrate the relative degradation was in the range of 3–6%. Annealing experiments

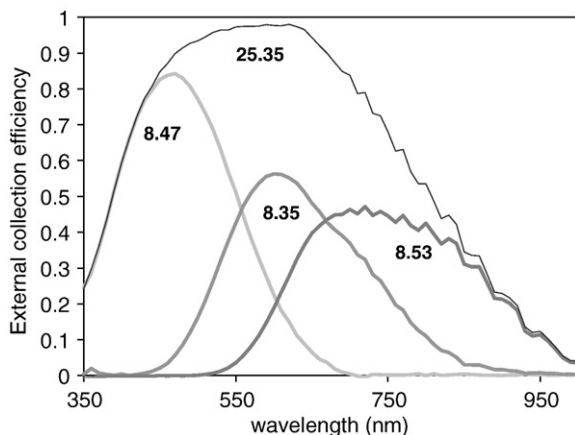


Fig. 5. Spectral response of a proto-Si:H/proto-SiGe:H/nc-Si:H triple junction solar cell on a textured back contact. The values indicated are the generated current densities.

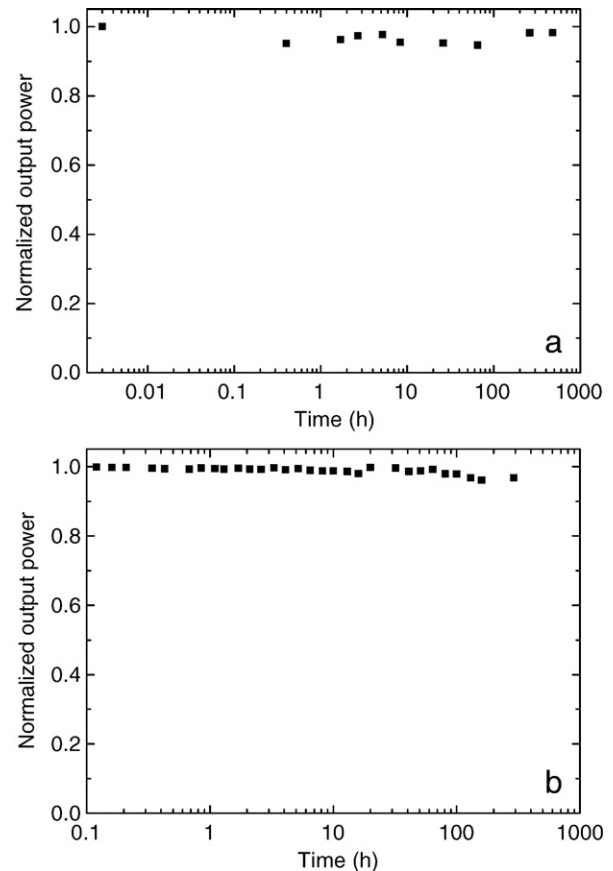


Fig. 6. a) Normalized light-induced performance evolution for a 2 μm thick nc-Si:H n-i-p cell, and b) Normalized light-induced performance evolution for a 2.5 μm thick proto-Si/proto-SiGe/nc-Si:H triple junction n-i-p solar cell.

at 150 $^{\circ}\text{C}$ showed that this degradation was reversible and therefore related to the Staebler–Wronski effect.

5. Conclusion

In summary, we have given two examples of how structures with nanoscale properties are used to considerably increase the performance of thin film silicon solar cells. First of all, a significant current enhancement is obtained by using textured Ag/ZnO back contacts instead of plain stainless steel. The textured interface acts as a diffuse scattering mirror, due to which the optical path in the cell is lengthened. Unfortunately, plasmon resonances at the rough Ag surface lead to parasitic absorption, which prevents taking full benefit of purely optical optimization of the roughness. We studied the *rms* roughness by 2D AFM and found that the response in the long-wavelength range can be correlated with the *rms* value, if it is weighted by a Power Spectral Density function and corrected for parasitic absorption due to surface particle plasmons. Optimized back reflectors lead to an enhancement of the photocurrent of as much as 50%. This has led to a stable efficiency of 8.5% for single junction nc-Si:H n-i-p cells, which is a record value for n-i-p cells with hot-wire deposited nc-Si:H i-layer.

The second large step forward is the use of multijunction (tandem or triple junction) cells, in which one of the cells is such

a nc-Si:H n-i-p cell. The nanocrystalline material in the i-layer contains 10–20 nm sized nanocrystals, together taking up 50% of the volume. Using this material in the bottom cell of a triple junction cell, in which the other two cells contain proto-SiGe and proto-Si as the active materials, has led to close to 11% efficiency. We used HWCVD to obtain the proto-Si:H and nc-Si:H absorber layers. Moreover, by using effective light trapping techniques and keeping all cell components very thin (total Si thickness is 2.5 μm), these triple cells are rather insensitive to light-induced defects and thus they are almost completely stable in operation.

Acknowledgments

We thank United Solar Ovonic LLC for providing stainless steel substrates with textured Ag/ZnO coatings. We also thank Gerard van der Mark and Arjen Bink for extensive technical assistance with the sputter tool. The research described in this paper was financially supported by the Netherlands Agency for Energy and the Environment (SenterNovem).

References

- [1] H. Curtins, N. Wyrsh, A.V. Shah, *Electron. Lett.* 23 (1987) 228.
- [2] A. Shah, J. Dutta, N. Wyrsh, K. Prasad, H. Curtins, F. Finger, A. Howling, Ch. Hollenstein, *Mater. Res. Soc. Symp. Proc.* 258 (1992) 15.
- [3] J.L. Dorier, C. Hollenstein, A.A. Howling, U. Kroll, *J. Vac. Sci. Technol., A* 10 (1992) 1048.
- [4] O. Vetterl, F. Finger, R. Carius, P. Hapke, L. Houben, O. Kluth, A. Lambertz, A. Mück, B. Rech, H. Wagner, *Sol. Energy Mater. Sol. Cells* 62 (2000) 97.
- [5] B. Schröder, U. Weber, H. Seitz, A. Ledermann, C. Mukherjee, *Thin Solid Films* 395 (2001) 298.
- [6] H. Matsumura, *Jpn. J. Appl. Phys.* 25 (1986) L949.
- [7] H. Matsumura, *J. Appl. Phys.* 65 (1989) 4396.
- [8] A.H. Mahan, J. Carapella, B.P. Nelson, R.S. Crandall, I. Balberg, *J. Appl. Phys.* 69 (1991) 6728.
- [9] R.E.I. Schropp, K.F. Feenstra, E.C. Molenbroek, H. Meiling, J.K. Rath, *Philos. Mag., B* 76 (1997) 309.
- [10] K.F. Feenstra, R.E.I. Schropp, W.F. van der Weg, *J. Appl. Phys.* 85 (1999) 6843.
- [11] R.E.I. Schropp, M.K. van Veen, C.H.M. van der Werf, D.L. Williamson, A.H. Mahan, *Proceedings of the 19th European Photovoltaic Solar Energy Conference, Paris (France), June 2004*, p. 1526.
- [12] J.J.H. Strengers, F.A. Rubinelli, J.K. Rath, R.E.I. Schropp, *Thin Solid Films* 501 (2006) 291.
- [13] M.K. van Veen, R.E.I. Schropp, *Appl. Phys. Lett.* 82 (2003) 287.
- [14] R.L. Stolk, H. Li, R.H. Franken, J.J.H. Strengers, C.H.M. van der Werf, J.K. Rath, R.E.I. Schropp, *J. Non-Cryst. Solids* 352 (2006) 1933.
- [15] B. Yan, G. Yue, J.M. Owens, J. Yang, S. Guha, 4th WCPEC, 7–12 May 2006, Waikoloa Village, Hawaii (USA).
- [16] A. Gordijn, R. Jimenez Zambrano, J.K. Rath, R.E.I. Schropp, *IEEE Trans. Electron Devices* 49 (2002) 949.
- [17] H. Li, R.H. Franken, R.L. Stolk, C.H.M. van der Werf, J.K. Rath, R.E.I. Schropp, *Thin Solid Films* 516 (2008) 755.
- [18] R.L. Stolk, J.J.H. Strengers, H. Li, R.H. Franken, C.H.M. van der Werf, J.K. Rath, R.E.I. Schropp, *Proc. 20th PVSEC*, 6–10 June 2005, p. 1655, Barcelona (Spain).
- [19] H. Li, R.L. Stolk, C.H.M. van der Werf, R.H. Franken, J.K. Rath, R.E.I. Schropp, *J. Non-Cryst. Solids* 352 (2006) 1941.
- [20] M.K. van Veen, Ph.D. thesis, Utrecht University, the Netherlands, 2003.
- [21] D. Williamson, *Mater. Res. Soc. Symp. Proc.* 557 (1999) 251.
- [22] M.K. van Veen, C.H.M. van der Werf, J.K. Rath, R.E.I. Schropp, *Thin Solid Films* 430 (2003) 216.
- [23] H. Franken, “Transparent Conducting Oxide Contacts and Textured Metal Back Reflectors for Thin Film Silicon Solar Cells”, Ph.D. Thesis, Utrecht University, 2006.
- [24] R.H. Franken, R.L. Stolk, H. Li, C.H.M. van der Werf, J.K. Rath, R.E.I. Schropp, *J. Appl. Phys.* 102 (2007) 014503.
- [25] S. Klein, F. Finger, R. Carius, O. Kluth, A.L. Baia Neto, H. Wagner, M. Stutzmann, *Proceedings of the 17th ECPVSEC, Munich, 2001*, p. 2965.
- [26] B. Schröder, M. Kupich, P. Kumar, D. Grunsky, *Thin Solid Films* 516 (2008) 722.
- [27] C. Niikura, Y. Poissant, M.E. Gueunier, J.P. Kleider, J.E. Bourée, *J. Non-Cryst. Solids* 299–302 (2002) 1179.
- [28] K. Mizuno, S. Ogawa, M. Okabe, T. Itoh, N. Yoshida, S. Nonomura, *Extended Abstracts of the 4th International Conference on Hot-Wire CVD (Cat-CVD) Process, Takayama, 2006*, HW4-023.
- [29] S. Klein, F. Finger, R. Carius, B. Rech, L. Houben, M. Luysberg, M. Stutzmann, *Mater. Res. Soc. Symp. Proc.* 715 (2002) A26.2.1.
- [30] M. Kupich, P. Kumar, R.O. Dusane, N. Schwender, D. Grunsky, B. Schröder, *Proceedings of the 20th European Photovoltaic Solar Energy Conf., Barcelona (Spain), June 2005*, p. 1679.
- [31] Y. Xu, A.H. Mahan, L.M. Gedvilas, R.C. Reedy, H. Branz, *Thin Solid Films* 501 (2006) 198.